

Harmonic Power-Flow Study of Hybrid AC/DC Grids with Converter-Interfaced Distributed Energy Resources

Johanna Kristin Maria Becker, Yihui Zuo, Mario Paolone
Distributed Electrical Systems Laboratory
École Polytechnique Fédérale de Lausanne
Lausanne, Switzerland
{johanna.becker, yihui.zuo, mario.paolone}@epfl.ch

Andreas Martin Kettner
PSI NEPLAN AG
Küsnacht (Zürich), Switzerland
andreas.kettner@neplan.ch

Abstract—As the share of *Converter-Interfaced Distributed Energy Resources* (CIDERS) in power distribution systems increases, hybrid AC/DC distribution systems are drawing more interest. Indeed, CIDERS usually rely on DC power and hybrid AC/DC grids with few *Network-Interfacing Converters* (NICs) are a promising solution to decrease installation costs and conversion losses compared to a pure AC grid. However, interactions between the AC and DC subsystem of a hybrid AC/DC grid can lead to undesirable amplification and propagation of harmonics. The authors of this paper have recently proposed a *Harmonic Power-Flow* (HPF) method that accurately represents the AC power flows including the coupling between different harmonics. The HPF framework is formulated through the mismatch equations of the nodal equations between the grid and the resource models and solved by a Newton Raphson algorithm. This paper updates the HPF method to model hybrid AC/DC grids interconnected through NICs. To this end, the model of the NICs and the resulting coupling between the AC and DC subsystems is included in the mismatch equations and the Jacobian matrix of the algorithm. The updated HPF method is applied to a typical hybrid AC/DC grid, and its accuracy is validated through detailed time-domain simulations with Simulink.

Index Terms—Hybrid AC/DC grid, converter-interfaced resources, AC/DC interactions, harmonic power-flow study.

I. INTRODUCTION

Modern power distribution systems are experiencing a large-scale integration of distributed energy resources. Since the majority of these resources rely on DC power, they need to be interfaced to the AC grid through AC/DC converters. Due to the potential to exploit synergies of the DC components of such *Converter-Interfaced Distributed Energy Resources* (CIDERS), the concept of DC microgrids has emerged. DC microgrids are promising in terms of eliminating redundant converter stages along with the associated installation cost and energy losses [1]. Since AC grids are still dominant in today's power system, it is not expected that they will

be replaced by DC grids entirely. Instead, so-called hybrid AC/DC grids are envisioned as a possible architecture to profit from the advantages of both types of systems [2]. In a hybrid AC/DC grid, the AC and DC subsystems are interconnected through so-called *Network-Interfacing Converters* (NICs). The interconnection of AC and DC grids can help to augment the reliability and stability of the entire system if adequate control schemes are used [3].

The presence of numerous CIDERS can cause high levels of harmonic distortions in power distribution systems [4]. Moreover, when interfacing subsystems composed of entire AC and DC grids, significant harmonic propagation between them is expected to occur [5]. In order to mitigate undesired amplification of harmonics in such cases, the appropriate design and tuning of the controllers of CIDERS and NICs is crucial [5]. To this end, accurate methods for the computation and analysis of harmonics and their propagation through CIDERS, NICs, and the grid are required.

Power-flow methods for the analysis of hybrid AC/DC grids have been studied extensively for transmission systems. In the literature, these methods are classified as *sequential* or *unified* algorithms. A sequential algorithm solves the AC and DC equations separately [6], while a unified algorithm solves the complete set of equations jointly [7]. In [8] and [7], power-flow analyses are performed for AC grids including HVDC links by means of a unified and sequential approach, respectively. A comparison of a unified and a sequential *Harmonic Power-Flow* (HPF) method for hybrid AC/DC grids including a single HVDC link is performed in [9].

A power-flow method for hybrid AC/DC grids on distribution system level is proposed in [10]. The method is formulated in a unified fashion and is capable of analysing entire DC grids as opposed to single HVDC links. To the best of the authors' knowledge, no generic and modular HPF study exists that allows the analysis of entire hybrid AC/DC grids while modelling in detail the harmonics in CIDERS and NICs.

The authors of this paper have recently proposed a framework for the HPF study of polyphase grids with a high share of CIDERS [11]–[13]. This method is generic, modular

This work was funded by the Schweizerischer Nationalfonds (SNF, Swiss National Science Foundation) via the National Research Programme NRP 70 "Energy Turnaround" (projects nr. 173661 and 197060) and by the Deutsche Forschungsgemeinschaft (DFG, German Research Foundation) via the Priority Programme DFG SPP 1984 "Hybrid and Multimodal Energy Systems" (project nr. 359982322).

and accurate and includes the coupling between harmonics. The models are described by linear time-periodic state-space models, which are transformed to the frequency domain by means of the Fourier analysis and Toeplitz matrices. The HPF problem is formulated based on the closed-loop transfer functions of the CIDERS and the hybrid nodal equations of the grid, and solved using the Newton Raphson method. The CIDER model proposed in [13] represents both the AC- and DC-side components and their controllers in detail.

This paper extends the HPF algorithm to be applicable to hybrid AC/DC grids. To this end, the model of the NICs which interfaces the AC and DC grids is derived as an extension of the generic CIDER model in [13]. Furthermore, the structure of the HPF method and the Jacobian matrix required for the Newton-Raphson algorithm are updated from the previous versions. More precisely, the Jacobian matrix is built through combination of the Jacobian matrices of the individual subsystems along with the respective coupling terms which are due to the NICs.

The rest of this paper is structured as follows. Section II gives a short summary of the time-domain model of a NIC and how it is obtained from the one of a CIDER as proposed in [13]. In Section III the node partition known from previous papers is refined for hybrid AC/DC grids. Furthermore, the harmonic-domain grid responses of the resources are shortly recalled from previous papers and introduced for the case of the NICs. Section IV shows the changes in the HPF algorithm for hybrid AC/DC grids compared to the previous versions. The HPF method for hybrid AC/DC grids is validated in Section V and the conclusions are drawn in Section VI.

II. MODEL OF A NETWORK-INTERFACING CONVERTER

NICs interconnect the AC and DC subsystems of a power grid. The structure of a NIC is similar to the one of a CIDER proposed in Section IV of [13]. Like a CIDER, a NIC consists of power hardware and control software.

In this paper, the generic power hardware is modeled by the structure in Fig. 1. It consists of an LCL filter on the AC side and a DC-link capacitor on the DC side. Note that, as compared to the CIDER in [13], a NIC has an additionally interface to the DC subsystem. Hence, the terminals of a NIC are characterized by the AC current i^{AC} and voltage v^{AC} , plus the DC current i^{DC} and voltage v^{DC} . The development of the time-domain state-space model of the power hardware including the DC-link capacitor is explained in detail in Section IV.A of [13].

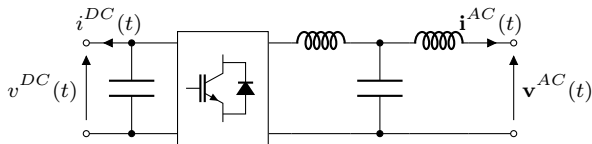


Fig. 1. Simplified representation of the power hardware of a NIC.

Two different types of control laws are considered for the NICs: regulation of either i) the DC-voltage and reactive

power or ii) the active and reactive power injected on the AC side. In this paper, these two types of resources are referred to as V_{DC}/Q -controlled NIC and P/Q -controlled NIC, respectively. The time-domain state-space model of the control software of a V_{DC}/Q -controlled NIC is shown in detail in Section IV.B of [13]. The control software of a P/Q -controlled NIC is identical to the one of the grid-following CIDER proposed in Section III.C of [12]. Further details on the derivations can be found in the respective references.

III. RESOURCE REPRESENTATION FOR HPF STUDIES

From the time-domain state-space models of the resources, one can derive the harmonic-domain grid response. For this purpose, the state-space models of power hardware and control software are first transformed to the harmonic domain by means of Fourier theor leading to Toeplitz matrices. Then, they are combined to form the closed-loop model of the resource. From this closed-loop model, the grid response of the resource is derived in the form of its harmonic transfer function. Further details about this procedure can be found in Section IV.B of [11].

A. Types of Resources and Partition of the Nodes

The specific grid response of a resource describes its behaviour as seen from the point of connection to the grid. A *grid-forming* resource controls the magnitude and frequency of the grid voltage at its point of connection. On the contrary, a *grid-following* resource controls the injected current with a specific phase displacement w.r.t. the fundamental component of the grid voltage at its point of connection. In line with these definitions, the set of all nodes \mathcal{N}^j of a subsystem j is partitioned into the disjoint sets \mathcal{S}^j and \mathcal{R}^j , where grid-forming resources $s \in \mathcal{S}^j$ and grid-following resources $r \in \mathcal{R}^j$ are connected, respectively:

$$\mathcal{N}^j = \mathcal{S}^j \cup \mathcal{R}^j, \quad \mathcal{S}^j \cap \mathcal{R}^j = \emptyset \quad (1)$$

In hybrid AC/DC grids, which consist of multiple subsystems, resources can be of single- or two-port type. Single-port devices possess a single input/output terminal associated with one specific subsystem. For instance, CIDERS and impedance loads previously employed in [12], [13] are single-port devices. Two-port devices are interconnections between two different subsystems. For example, the NICs introduced in Section II have two ports (i.e., one each on the AC and DC side). Following this reasoning, for each subsystem the sets \mathcal{R}^j and \mathcal{S}^j are further subdivided into two disjoint sets:

$$\mathcal{R}^j = \mathcal{R}_1^j \cup \mathcal{R}_2^j, \quad \mathcal{R}_1^j \cap \mathcal{R}_2^j = \emptyset \quad (2)$$

$$\mathcal{S}^j = \mathcal{S}_1^j \cup \mathcal{S}_2^j, \quad \mathcal{S}_1^j \cap \mathcal{S}_2^j = \emptyset \quad (3)$$

where \mathcal{R}_1^j and \mathcal{S}_1^j consist of all grid-forming and grid-following single-port resources (e.g., CIDERS), respectively and \mathcal{R}_2^j and \mathcal{S}_2^j represent the nodes where the two-port resources (i.e., NICs) are connected. The node partition of such a generic subsystem j is shown in Fig. 2a. In Fig. 2b the example of a hybrid AC/DC grid consisting of one AC

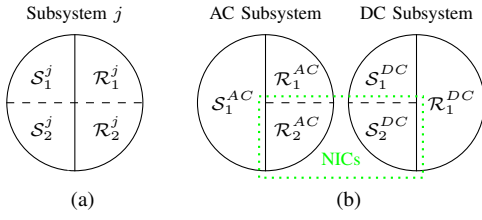


Fig. 2. Partition of the nodes for a generic subsystem j (Fig. 2a) and for a hybrid AC/DC grid with NICs connecting \mathcal{R}_2^{AC} and \mathcal{S}_2^{DC} (Fig. 2b).

and one DC subsystem is shown. In this example the two-port devices are purely composed of NICs that connect \mathcal{R}_2^{AC} and \mathcal{S}_2^{DC} . Hence, the sets \mathcal{S}_2^{AC} and \mathcal{R}_2^{DC} are empty.

B. Grid Response of Single-Port Resources

As previously stated, the grid response of a single-port resource defines either the voltage in function of the current or vice versa. As it was introduced in Section II.C of [13], the grid responses of grid-forming and grid-following CIDERs can be expressed as follows:

$$s \in \mathcal{S}_1^j : \hat{\mathbf{V}}_s^j = \hat{\mathbf{Y}}_s(\hat{\mathbf{I}}_s^j, \hat{\mathbf{W}}_{\sigma,s}, \hat{\mathbf{Y}}_{o,s}) \quad (4)$$

$$r \in \mathcal{R}_1^j : \hat{\mathbf{I}}_r^j = \hat{\mathbf{Y}}_r(\hat{\mathbf{V}}_r^j, \hat{\mathbf{W}}_{\sigma,r}, \hat{\mathbf{Y}}_{o,r}) \quad (5)$$

where $\hat{\mathbf{V}}_s^j$ and $\hat{\mathbf{I}}_s^j$ are the column vectors of the Fourier coefficients of the terminal voltages $\mathbf{v}_s^j(t)$ and currents $\mathbf{i}_s^j(t)$, respectively, of the grid-forming resources. Similarly, $\hat{\mathbf{V}}_r^j$ and $\hat{\mathbf{I}}_r^j$ represent the column vectors of the terminal voltages and currents of the grid-following resources. The inputs $\hat{\mathbf{W}}_{\sigma,s}$ and $\hat{\mathbf{Y}}_{o,s}$ represent the setpoints and the operating points, respectively, of the CIDERs. The latter is needed in case a linearization was performed in the derivation of the CIDER model, as presented in Section II.C of [13]. It is worth noting that this representation of the grid response is generic (e.g., it also applies to passive loads) and that it is valid irrespective of the type of grid it is connected to (i.e., AC or DC). For further details on the derivation of the grid response, please refer to Section II.C of [13].

C. Grid Response of Two-Port Resources

The grid response of a two-port device is described by two pairs of electrical quantities (i.e., voltages and currents at both ports). It is important to note that a NIC cannot exhibit grid-forming and grid-following behaviour arbitrarily at each port as the corresponding circuit equations cannot be overdetermined. To be more precise, one cannot simultaneously control the voltages or currents at both ports. By consequence, if one port exhibits a grid-forming behaviour, the other must exhibit a grid-following behaviour.

Typically, NICs perform grid-forming control on the DC side and grid-following control on the AC side¹. Thus, a NIC can be seen as a branch $m = (r, s)$ between two nodes

¹In theory, it is possible to perform grid-forming control on the AC side and grid-following control on the DC side. In practice, this configuration is not employed to the best of the authors' knowledge.

$r \in \mathcal{R}_2^{AC}$ and $s \in \mathcal{S}_2^{DC}$ (i.e., $\mathcal{M} \subseteq \mathcal{R}_2^{AC} \times \mathcal{S}_2^{DC}$). The grid response of a NIC $m = (r, s) \in \mathcal{M}$ is described by

$$[\hat{\mathbf{I}}_r^{AC}, \hat{\mathbf{V}}_s^{DC}] = \hat{\mathbf{Y}}_m(\hat{\mathbf{V}}_r^{AC}, \hat{\mathbf{I}}_s^{DC}, \hat{\mathbf{W}}_{\sigma,m}, \hat{\mathbf{Y}}_{o,m}) \quad (6)$$

As for the case of CIDERs, $\hat{\mathbf{W}}_{\sigma,m}$ and $\hat{\mathbf{Y}}_{o,m}$ denote the setpoint and operating point, respectively.

IV. HPF ALGORITHM FOR HYBRID AC/DC GRIDS

The HPF framework proposed in [11] describes AC power systems by two sets of nodal equations. Namely, the nodal quantities are expressed from the point of view of the grid and the resources, respectively. Recall from Section III the partition of the nodes of each subsystem into the sets \mathcal{S}^j and \mathcal{R}^j . The unknowns of the HPF problem are the nodal injected currents at the nodes \mathcal{S}^j and the nodal phase-to-ground voltages at the nodes \mathcal{R}^j (i.e., the quantities that are not regulated by the respective type of resource). The nodal equations of a hybrid AC/DC grid are obtained as the combination of the nodal equations of all subsystems.

A. Mismatch Equations

The nodal equations for each subsystem j seen from the grid are formulated using hybrid parameters:

$$\hat{\mathbf{V}}_S^j = \hat{\mathbf{H}}_{S \times S}^j \hat{\mathbf{I}}_S^j + \hat{\mathbf{H}}_{S \times \mathcal{R}}^j \hat{\mathbf{V}}_{\mathcal{R}}^j \quad (7)$$

$$\hat{\mathbf{I}}_{\mathcal{R}}^j = \hat{\mathbf{H}}_{\mathcal{R} \times S}^j \hat{\mathbf{I}}_S^j + \hat{\mathbf{H}}_{\mathcal{R} \times \mathcal{R}}^j \hat{\mathbf{V}}_{\mathcal{R}}^j \quad (8)$$

where $\hat{\mathbf{H}}_{S \times S}^j$, $\hat{\mathbf{H}}_{S \times \mathcal{R}}^j$, $\hat{\mathbf{H}}_{\mathcal{R} \times S}^j$ and $\hat{\mathbf{H}}_{\mathcal{R} \times \mathcal{R}}^j$ are the blocks of the hybrid matrix $\hat{\mathbf{H}}^j$ associated with \mathcal{S}^j and \mathcal{R}^j . $\hat{\mathbf{I}}_S^j$ and $\hat{\mathbf{V}}_{\mathcal{R}}^j$ are the column vectors of all nodal injected currents at the nodes \mathcal{S}^j and all nodal phase-to-ground voltages at the nodes \mathcal{R}^j , respectively. For further details, please see Section III of [11].

The HPF problem is given by the mismatch equations between (7)–(8) on the one hand and the grid responses of the resources (4)–(5) and (6) on the other hand. At the equilibrium, these mismatches must be zero. Thus, at the nodes where single-port resources are connected:

$$\Delta \hat{\mathbf{V}}_{S_1}^j(\hat{\mathbf{I}}_S^j, \hat{\mathbf{V}}_{\mathcal{R}}^j, \hat{\mathbf{W}}_{\sigma,S_1}^j, \hat{\mathbf{Y}}_{o,S_1}^j) = \mathbf{0} \quad (9)$$

$$\Delta \hat{\mathbf{I}}_{\mathcal{R}_1}^j(\hat{\mathbf{I}}_S^j, \hat{\mathbf{V}}_{\mathcal{R}}^j, \hat{\mathbf{W}}_{\sigma,\mathcal{R}_1}^j, \hat{\mathbf{Y}}_{o,\mathcal{R}_1}^j) = \mathbf{0} \quad (10)$$

Notably, this formulation corresponds to the one introduced in Section III of [13]. At the nodes where two-port resources are connected, the argument of the mismatch equations has to be expanded to account for the quantity of the second terminal of the NICs. Thus,

$$\Delta \hat{\mathbf{V}}_{S_2}^{DC}(\hat{\mathbf{I}}_S^{DC}, \hat{\mathbf{V}}_{\mathcal{R}}^{DC}, \hat{\mathbf{V}}_{\mathcal{R}_2}^{AC}, \hat{\mathbf{W}}_{\sigma,S_2}^{DC}, \hat{\mathbf{Y}}_{o,S_2}^{DC}) = \mathbf{0} \quad (11)$$

$$\Delta \hat{\mathbf{I}}_{\mathcal{R}_2}^{AC}(\hat{\mathbf{I}}_S^{AC}, \hat{\mathbf{V}}_{\mathcal{R}}^{AC}, \hat{\mathbf{I}}_{S_2}^{DC}, \hat{\mathbf{W}}_{\sigma,\mathcal{R}_2}^{AC}, \hat{\mathbf{Y}}_{o,\mathcal{R}_2}^{AC}) = \mathbf{0} \quad (12)$$

where $\hat{\mathbf{V}}_{S_2}^{AC}$ and $\hat{\mathbf{I}}_{S_2}^{DC}$ represent the coupling between the two subsystems. This system of equations can be solved using the Newton-Raphson algorithm. To this end, the Jacobian matrix of the equations is required.

B. Jacobian Matrix

The Jacobian matrix $\hat{\mathbf{J}}$ required for the Newton-Raphson algorithm is derived as the difference between the Jacobian matrices of the equations related to the resources $\hat{\mathbf{J}}^{RSC}$ and the grid $\hat{\mathbf{J}}^{GRD}$, respectively. That is,

$$\hat{\mathbf{J}} = \hat{\mathbf{J}}^{RSC} - \hat{\mathbf{J}}^{GRD} \quad (13)$$

$\hat{\mathbf{J}}^{GRD}$ is composed of the partial derivatives of the grid equations in (7)–(8) w.r.t. $\hat{\mathbf{I}}_S^j$ and $\hat{\mathbf{V}}_{\mathcal{R}}^j$, respectively. More precisely, it is composed of the hybrid parameters of the AC and DC subsystem:

$$\hat{\mathbf{J}}^{GRD} = \begin{bmatrix} \hat{\mathbf{H}}_{S \times S}^{AC} & \hat{\mathbf{H}}_{S \times \mathcal{R}}^{AC} & \mathbf{0} & \mathbf{0} \\ \hat{\mathbf{H}}_{\mathcal{R} \times S}^{AC} & \hat{\mathbf{H}}_{\mathcal{R} \times \mathcal{R}}^{AC} & \mathbf{0} & \mathbf{0} \\ \mathbf{0} & \mathbf{0} & \hat{\mathbf{H}}_{S \times S}^{DC} & \hat{\mathbf{H}}_{S \times \mathcal{R}}^{DC} \\ \mathbf{0} & \mathbf{0} & \hat{\mathbf{H}}_{\mathcal{R} \times S}^{DC} & \hat{\mathbf{H}}_{\mathcal{R} \times \mathcal{R}}^{DC} \end{bmatrix} \quad (14)$$

Notably, this matrix has a block-diagonal structure, and exhibits no coupling between AC and DC quantities.

$\hat{\mathbf{J}}^{RSC}$ is composed of the partial derivatives of the grid responses in (4)–(5) and (6) w.r.t. $\hat{\mathbf{I}}_S^j$ and $\hat{\mathbf{V}}_{\mathcal{R}}^j$, respectively. The following notation is introduced in the following for the sake of conciseness:

$$\partial_{S_k}^j = \frac{\partial}{\partial \hat{\mathbf{I}}_{S_k}^j}, \quad \partial_{\mathcal{R}_k}^j = \frac{\partial}{\partial \hat{\mathbf{V}}_{\mathcal{R}_k}^j} \quad (15)$$

$\hat{\mathbf{J}}^{RSC}$ is depicted in (16). At nodes with single-port resources, the corresponding blocks of the Jacobian matrix exhibit a diagonal structure, since a resource influences only the quantity at its point of connection. These terms associated with the AC and DC single-port resources are highlighted in blue and red, respectively, in (16). At nodes with two-port resources (i.e., where NICs are connected), off-diagonal terms appear in the Jacobian matrix. They describe the coupling between the AC and DC port of the NICs, respectively, as well as between the AC and DC subsystems. These terms are highlighted in green in (16).

Details on the derivation of the partial derivatives in (14) and (16) can be found in Section V.B of [11].

Using the aforesaid expression for the mismatch equations and the Jacobian matrix, the HPF problem can be solved by means of the Newton-Raphson algorithm as described in Section III of [13].

V. VALIDATION

A. Methodology and Key Performance Indicators

The HPF algorithm for hybrid AC/DC grids is validated on an extension of the benchmark AC microgrid proposed in [14]. More specifically, the benchmark system is extended by a DC grid following the example of [15]. As depicted in Fig. 3 the AC and DC subsystems are interfaced through NICs at the nodes N15-18 on the AC side and N19-22 on the DC side. Their specifications are given in Table I. The AC subsystem is composed of a feeding substation at node N1, seven grid-following CIDERS at nodes N5, N9, N11 and

TABLE I
PARAMETERS OF NETWORK-INTERFACING CONVERTERS.

AC Node	DC Node	P	Q	V_{DC}	Type
N15	N19	-	9.9 kVar	900 V	V_{DC}/Q
N16	N20	30.0 kVar	9.9 kVar	-	P/Q
N17	N21	-25.0 kVar	8.2 kVar	-	P/Q
N18	N22	30.0 kVar	9.9 kVar	-	P/Q

TABLE II
PARAMETERS OF THE GRID-FOLLOWING RESOURCES AND LOADS.

Node	S	pf	Type
N05	-20.6 kW	0.97	P/Q
N09-1	49.1 kW	0.95	P/Q
N09-2	2.0 kW	1.00	P/Q
N11-1	11.2 kW	0.95	P/Q
N11-2	9.1 kW	0.95	P/Q
N13-1	10.5 kW	0.95	P/Q
N13-2	-10.0 kW	1.00	P/Q
N03	-20.0 kW	1.00	Z
N14	-15.0 kW	1.00	Z
N23	5.0 kW	-	I
N25	10.0 kW	-	I
N26	5.0 kW	-	I
N24	-8.0 kW	-	Z

N13 and two passive loads at nodes N3 and N14. The DC subsystem consists of three current sources at nodes N23 and N25-26, and a passive load at node N24. The references of the resources are given in Table II. The feeding substation of the AC subsystem is modelled as a TE described by parameters depicted in Table III. The TE injects harmonics with levels shown in Table IV based on [16]. The line parameters of the AC and DC subsystems are given in Table V.

The validation of the HPF algorithm is performed through *Time-Domain Simulations* (TDS) in Simulink. To this end, the system in Fig. 3 is replicated using the models of the CIDERS in [13]. The Matlab code of the HPF method is updated to account for hybrid AC/DC grids. For the TDS, a *Discrete Fourier Transform* (DFT) over 5 periods of the fundamental frequency in steady state is performed. All signals are normalized w.r.t. the base power $P_b = 50$ kW and base voltage $V_b = 230$ V-RMS.

To assess the accuracy of the HPF method compared to the TDS so-called *Key Performance Indicators* (KPIs) are defined. More specifically, the errors of the harmonic phasors between the DFT of the TDS and the results of the HPF are derived. Let the Fourier coefficient of a three-phase electrical quantity (i.e., voltage or current) be denoted as \mathbf{X}_h . Then, the KPIs are defined as:

$$e_{\text{abs}}(\mathbf{X}_h) := \max_p \left| |X_{h,p,HPF}| - |X_{h,p,TDS}| \right| \quad (17)$$

$$e_{\text{arg}}(\mathbf{X}_h) := \max_p \left| \angle X_{h,p,HPF} - \angle X_{h,p,TDS} \right| \quad (18)$$

In short, $e_{\text{abs}}(\mathbf{X}_h)$ and $e_{\text{arg}}(\mathbf{X}_h)$ represent the maximum absolute errors over all phases $p \in \mathcal{P}$ in magnitude and angle, respectively.

$$\hat{\mathbf{j}}^{RSC} = \begin{bmatrix} \underbrace{\partial_{S_1}^{AC} \hat{\mathbf{V}}_{S_1}^{AC}}_{S^{AC}} & \underbrace{\mathbf{0} \quad \mathbf{0}}_{R^{AC}} & \underbrace{\mathbf{0} \quad \mathbf{0}}_{S^{DC}} & \underbrace{\mathbf{0}}_{R^{DC}} \\ \mathbf{0} & \partial_{R_1}^{AC} \hat{\mathbf{I}}_{R_1}^{AC} & \mathbf{0} & \mathbf{0} \\ \mathbf{0} & \mathbf{0} & \partial_{R_2}^{AC} \hat{\mathbf{I}}_{R_2}^{AC} & \mathbf{0} \\ \mathbf{0} & \mathbf{0} & \mathbf{0} & \partial_{S_1}^{DC} \hat{\mathbf{V}}_{S_1}^{DC} \\ \mathbf{0} & \partial_{R_2}^{DC} \hat{\mathbf{V}}_{S_2}^{DC} & \mathbf{0} & \mathbf{0} \\ \mathbf{0} & \mathbf{0} & \mathbf{0} & \partial_{R_1}^{DC} \hat{\mathbf{I}}_{R_1}^{DC} \end{bmatrix} \quad (16)$$

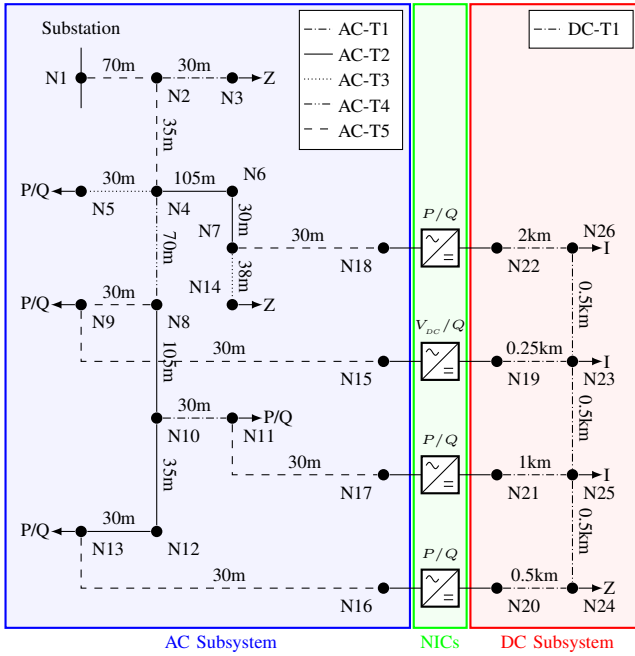


Fig. 3. Schematic diagram of the test system, which is based on the CIGRÉ low-voltage benchmark microgrid [14] (blue box) and interfaced through NICs (green box) to the DC subsystem (red box), parameters given in Table I. The resources are composed of constant impedance loads (Z), constant power loads (P/Q), and constant current sources (I), parameters given in Table II.

TABLE III
SHORT-CIRCUIT PARAMETERS OF THE THÉVENIN EQUIVALENT.

Parameter	Value	Description
V_n	230 V-RMS	Nominal voltage
S_{sc}	630 kW	Short-circuit power
$ Z_{sc} $	16.3 m Ω	Short-circuit impedance
R_{sc}/X_{sc}	0.125	Resistance-to-reactance ratio

B. Results and Discussions

In Fig. 4 the accuracy of the HPF algorithm for hybrid AC/DC grids is compared to the TDS in Simulink. The highest errors at every harmonic frequency and over all nodes and phases for nodal voltages and injected currents are shown for

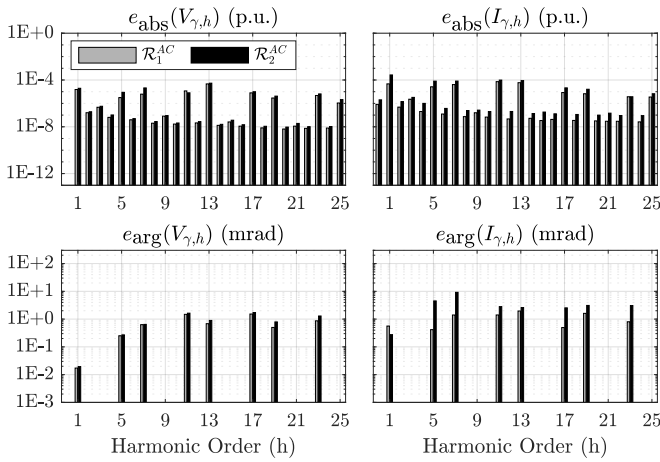
TABLE IV
HARMONIC VOLTAGES OF THE THÉVENIN EQUIVALENT (SEE [16]).

h	$ V_{TE,h} $	$\angle V_{TE,h}$
1	1.0 p.u.	0 rad
5	6.0 %	$\pi/8$ rad
7	5.0 %	$\pi/12$ rad
11	3.5 %	$\pi/16$ rad
13	3.0 %	$\pi/8$ rad
17	2.0 %	$\pi/12$ rad
19	1.5 %	$\pi/16$ rad
23	1.5 %	$\pi/16$ rad

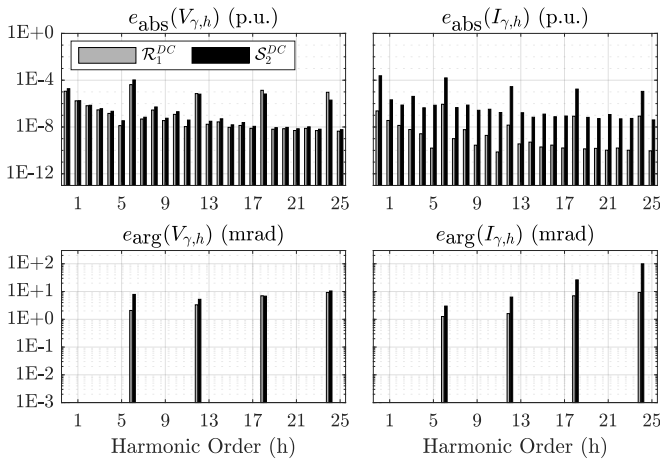
TABLE V
AC (+/-/0) AND DC PARAMETERS OF THE LINES.

ID	$R_{+/-/0}$ or R	$L_{+/-/0}$ or L	$C_{+/-/0}$ or C
AC-T1	3.30 Ω /km	0.45 mH/km	150 nF/km
AC-T2	1.21 Ω /km	0.42 mH/km	230 nF/km
AC-T3	0.78 Ω /km	0.40 mH/km	210 nF/km
AC-T4	0.55 Ω /km	0.39 mH/km	260 nF/km
AC-T5	0.27 Ω /km	0.38 mH/km	320 nF/km
DC-T1	0.08 Ω /km	0.28 mH/km	292 nF/km

the two subsystems independently. In Fig. 4a the errors are shown for the set of all CIDERS and NICs, as well as the passive impedance loads. For the DC subsystem, the set of grid-forming (i.e., including the DC quantities of the NICs) and grid-following nodes is shown. The maximum errors regarding the voltages and currents occur in both subsystems in the nodes where the NICs are connected. More precisely, the maximum errors in magnitude and phase for the voltages are $e_{\text{abs}}(\mathbf{V}_{13}) = 5.37\text{E-}5$ p.u. and $e_{\text{arg}}(\mathbf{V}_{17}) = 1.7$ mrad in the AC subsystem and $e_{\text{abs}}(\mathbf{V}_6) = 1.05\text{E-}4$ p.u. and $e_{\text{arg}}(\mathbf{V}_{24}) = 10.5$ mrad in the DC subsystem, respectively. The maximum errors w.r.t. current magnitude and angle are $e_{\text{abs}}(\mathbf{I}_1) = 2.71\text{E-}4$ p.u. and $e_{\text{arg}}(\mathbf{I}_7) = 9.2$ mrad in the AC subsystem and $e_{\text{abs}}(\mathbf{I}_0) = 2.38\text{E-}4$ p.u. and $e_{\text{arg}}(\mathbf{I}_{24}) = 99.5$ mrad in the DC subsystem, respectively. The obtained errors for both subsystems are lower than the accuracy of standard measurement equipment (i.e., they are unobservable in practice). Thus, the accuracy of the HPF method for hybrid AC/DC grids is validated.



(a)



(b)

Fig. 4. Results of the validation of the AC (Fig. 4a) and DC subsystem (Fig. 4b). The grid-following CIDERS (\mathcal{R}_1^{AC}) and the AC side of the NICs (\mathcal{R}_2^{AC}), as well as the DC-side resources (\mathcal{R}_1^{DC}) and the DC side of the NICs (\mathcal{S}_2^{DC}) are shown. The plots show the maximum absolute errors over all nodes and phases, for voltages (left column) and currents (right column), in magnitude (top row) and phase (bottom row).

VI. CONCLUSIONS

This paper proposes an HPF algorithm for the analysis of hybrid AC/DC grids, which is an extension of the HPF algorithm for AC grids introduced in [11]–[13]. In hybrid grids, the AC and DC subsystems are interconnected through NICs. Those NICs have two ports: i.e., one on the AC side and one on the DC side. To include this behaviour into the previously developed HPF framework, resources are separated into single-port and two-port devices. Single-port resources (e.g., CIDERS) lie within one single subsystem, while two-port resources (i.e., NICs) interconnect two different subsystems. The HPF algorithm is formulated based on the mismatch equations of the nodal equations as seen from the grid and the resources, respectively, and solved via the Newton-Raphson method. In order to include the NICs and the DC subsystem, the structure of the Jacobian matrix of

the HPF is suitably modified. More precisely, it is written as the difference between the Jacobian matrices associated with the grid and the resource equations, respectively. The former matrix has a block-diagonal structure, and exhibits no coupling between AC and DC quantities. The latter matrix does feature coupling terms (i.e., non-zero off-diagonal blocks), which are due to the two-port nature of the NICs. The HPF method for hybrid AC/DC grids is validated through TDS in Simulink. The errors observed in these simulations demonstrate the high accuracy of the HPF w.r.t. the TDS. The largest observed errors are $2.71\text{E-}4$ p.u. w.r.t. current magnitude, $1.05\text{E-}4$ p.u. w.r.t. voltage magnitude, and 99.5 mrad w.r.t. phase (at the edge of the modelled frequency window). This demonstrates that the proposed HPF method for hybrid AC/DC grids can accurately analyze the interaction of harmonics between entire AC and DC subsystems.

REFERENCES

- [1] N. Eghtedarpour and E. Farjah, “Power control and management in a hybrid ac/dc microgrid,” *IEEE Trans. on Smart Grid*, vol. 5, no. 3, pp. 1494–1505, 2014.
- [2] F. Nejabatkhah and Y. W. Li, “Overview of power management strategies of hybrid ac/dc microgrid,” *IEEE Trans. on Power Electron.*, vol. 30, no. 12, pp. 7072–7089, 2014.
- [3] M. N. Ambia, A. Al-Durra, and S. Mueeen, “Centralized power control strategy for ac-dc hybrid micro-grid system using multi-converter scheme,” in *IECON 2011-37th Annual Conference of the IEEE Industrial Electronics Society*. IEEE, 2011, pp. 843–848.
- [4] J. Enslin and P. Heskes, “Harmonic interaction between a large number of distributed power inverters and the distribution network,” *IEEE Trans. Power Electron.*, vol. 19, no. 6, pp. 1586–1593, 2004.
- [5] F. Nejabatkhah *et al.*, “Power quality control of smart hybrid ac/dc microgrids: An overview,” *Ieee access*, vol. 7, pp. 52 295–52 318, 2019.
- [6] J. Beerten, S. Cole, and R. Belmans, “Generalized steady-state vsc mtcd model for sequential ac/dc power flow algorithms,” *IEEE Trans. on Power Sys.*, vol. 27, no. 2, pp. 821–829, 2012.
- [7] M. Baradar and M. Ghandhari, “A multi-option unified power flow approach for hybrid ac/dc grids incorporating multi-terminal vsc-hvdc,” *IEEE Trans. on Power Sys.*, vol. 28, no. 3, pp. 2376–2383, 2013.
- [8] J. Beerten, S. Cole, and R. Belmans, “A sequential ac/dc power flow algorithm for networks containing multi-terminal vsc hvdc systems,” in *IEEE PES General Meeting*. IEEE, 2010, pp. 1–7.
- [9] B. Smith and J. Arrillaga, “Power flow constrained harmonic analysis in ac-dc power systems,” *IEEE Trans. on Power Sys.*, vol. 14, no. 4, pp. 1251–1261, 1999.
- [10] K. Murari *et al.*, “A network-topology-based approach for the load-flow solution of ac-dc distribution system with distributed generations,” *IEEE Trans. on Ind. Informatics*, vol. 15, no. 3, pp. 1508–1520, 2018.
- [11] A. M. Kettner *et al.*, “Harmonic power-flow study of polyphase grids with converter-interfaced distributed energy resources—part i: Modeling framework and algorithm,” *IEEE Trans. Smart Grid*, vol. 13, no. 1, pp. 458–469, 2021.
- [12] J. K. M. Becker *et al.*, “Harmonic power-flow study of polyphase grids with converter-interfaced distributed energy resources—part ii: Model library and validation,” *IEEE Trans. Smart Grid*, vol. 13, no. 1, pp. 470–481, 2021.
- [13] —, “Modelling of ac/dc interactions of converter-interfaced resources for harmonic power-flow studies in microgrids,” *IEEE Trans. Smart Grid*, 2022.
- [14] S. Papathanassiou, N. Hatziaargyriou, K. Strunz *et al.*, “A benchmark low voltage microgrid network,” in *Proceedings of the CIGRE symposium: power systems with dispersed generation*, 2005, pp. 1–8.
- [15] W. Lambrechts and M. Paolone, “Linear recursive state estimation of hybrid and unbalanced ac/dc micro-grids using synchronized measurements,” *IEEE Trans. on Smart Grid*, 2022.
- [16] “Voltage characteristics of electricity supplied by public distribution networks,” British Standards Institution, London, UK, Std. BS-EN-50160:2000, 2000.